Probing the impact of material properties of core-shell SiO2@TiO2 spheres on the plasma-catalytic CO2 dissociation using a packed bed DBD plasma reactor

Peer-reviewed author version

KALIYAPPAN, Periyasamy; PAULUS, Andreas; D'HAEN, Jan; SAMYN, Pieter; Uytdenhouwen, Yannick; Hafezkhiabani, Neda; Bogaerts, Annemie; Meynen, Vera; ELEN, Ken; HARDY, An & VAN BAEL, Marlies (2021) Probing the impact of material properties of core-shell SiO2@TiO2 spheres on the plasma-catalytic CO2 dissociation using a packed bed DBD plasma reactor. In: Journal of CO2 Utilization, 46 (Art N° 101468).

DOI: 10.1016/j.jcou.2021.101468
Handle: http://hdl.handle.net/1942/33462

Probing the impact of material properties of core-shell SiO_2@TiO_2 spheres on the plasma-catalytic CO_2 dissociation using a packed bed DBD plasma reactor

Periyasamy Kaliyappan[a], Andreas Paulus[a,g], Jan D'Haen[b], Pieter Samyn[c], Yannick Uytdenhouwen[f], Neda Hafezkhiabani[f], Annemie Bogaerts[f], Vera Meynen[d,e], Ken Elen[a,g], An Hardy[a,g] and Marlies K. Van Bael[a,g,*]

[a] Hasselt University, Institute for Materials Research (imo-imomec and Energyville), Materials Chemistry, DESINe group, Agoralaan Building D, 3590 Diepenbeek, Belgium

[b] Hasselt University, Institute for Materials Research (imo-imomec), Materials Physics, ELPHYC group, Wetenschapspark 1, 3590 Diepenbeek, Belgium

[c] Hasselt University, Institute for Materials Research (imo-imomec), Materials Chemistry, ACC group, Agoralaan Gebouw D, 3590 Diepenbeek, Belgium

[d] University of Antwerp, Department of Chemistry, Laboratory of Adsorption & Catalysis (LADCA), Universiteitsplein 1, 2610 Wilrijk, Belgium

[e] Flemish Institute of Technological Research (VITO), Boeretang 200, 2400 Mol, Belgium

[f] University of Antwerp, Department of Chemistry, Research group PLASMANT, Universiteitplein 1, 2610 Wilrijk, Belgium

[g] IMEC vzw, IMOMEC, Wetenschapspark 1, 3590 Diepenbeek, Belgium

* Corresponding author.

E-mail address: marlies.vanbael@uhasselt.be

Abstract

Plasma catalysis, a promising technology for conversion of CO_2 into value-added chemicals near room temperature, is gaining increasing interest. A dielectric barrier discharge (DBD) plasma has attracted attention due to its simple design and operation at near ambient conditions, ease to implement catalysts in the plasma zone and upscaling ability to industrial applications. To improve its main drawbacks, being relatively low conversion and energy efficiency, a packing

material is used in the plasma discharge zone of the reactor, sometimes decorated by a catalytic material. Nevertheless, the extent to which different properties of the packing material influence plasma performance is still largely unexplored and unknown. In this study, the particular effect of synthesis induced differences in the morphology of a TiO_2 shell covering a SiO_2 core packing material on the plasma conversion of CO_2 is studied. TiO_2 has been successfully deposited around 1.6-1.8 mm sized SiO_2 spheres by means of spray coating, starting from aqueous citratoperoxotitanate(IV) precursors. Parameters such as concentration of the Ti(IV) precursor solutions and addition of a binder were found to affect the shells' properties and surface morphology and to have a major impact on the CO_2 conversion in a packed bed DBD plasma reactor. Core-shell SiO_2@TiO_2 obtained from 0.25M citratoperoxotitante(IV) precursors with the addition of a LUDOX binder showed the highest CO_2 conversion 37.7% (at a space time of 70 s corresponding to an energy efficiency of 2%) and the highest energy efficiency of 4.8% (at a space time of 2.5 s corresponding to a conversion of 3%).

Keywords

Plasma catalysis; CO_2 splitting; DBD plasma; core-shell SiO_2@TiO_2 spheres; solution deposition

1. INTRODUCTION

Carbon dioxide (CO_2) is considered as one of the main contributors to global warming and concomitant climate change. Continuous consumption of fossil fuels for energy, transportation and some specific industrial processes is responsible for the gradual increase in the atmosphere's CO_2 concentration [1]. The unavoidable excess CO_2 in the atmosphere, which cannot be prevented, can be mitigated by its capture and storage [2]. Even though CO_2 capture and storage can play a role in lowering the amount of CO_2 in the atmosphere, the technology to achieve this is still restricted by high investment costs and uncertainty of potential long-term storage [3, 4]. Utilization of CO_2 by transforming it into value-added chemicals has gained significant attention in view of a future sustainable carbon-neutral economy in chemical and energy industries [4-6]. Several methods have been put forward to convert CO_2 into value-added chemicals, such as dry reforming of CH_4 [7-9], CO_2 dissociation [10, 11], or CO_2 hydrogenation to methanol [12], hydrocarbons [13, 14] or formaldehyde [15]. Direct splitting of pure CO_2 into CO and O_2 is an industrially important process, whereby CO is used as feedstock for other value-added products [16, 17]. The direct splitting of CO_2 into CO and O_2 is however a highly

endothermic reaction (ΔH_{298K} = 279.8 kJ/mol) due to the large amount of energy required to break the C=O bonds [18]. In conventional thermal catalysis, dissociation of CO_2 is achieved at 2000 K with low conversion rate (<1%). The highest CO_2 conversion (60%) was attained at extremely high temperature (3000-3500 K) [19, 20]. Non-thermal plasma (NTP) catalysis is an attractive alternative for conventional thermal catalysis, which activates CO_2 at near ambient conditions [21]. In a plasma, reactive species like electrons, ions, radicals and excited species are obtained by applying a high voltage to a gas. This provides energy, mainly to the light electrons, in the range of 1-10 eV (~ 10,000-100,000 K) [22], which is enough to break the C=O bond at ambient conditions (bond dissociation energy for CO_2 is 5.5 eV). The most commonly used plasma types for CO_2 conversion by direct splitting are microwave (MW) [23-25], gliding arc (GA) [26-28] and dielectric barrier discharge (DBD) plasma's [10, 11, 29-32], each with its own benefits and drawbacks. DBD reactors are well-known for their simple, robust design and relatively easy scalability towards industrial applications [33]. Their major advantage is their operation near room temperature and pressure and the possibility to implement materials in the plasma zone that can provide physical and possibly catalytic enhancements of the plasma processes.

Although plasma alone can convert CO_2 into CO, the main drawback of a DBD plasma is the low conversion and energy efficiency. It can be improved by the introduction of (catalyst) packing materials in the DBD reactor [34]. Recent studies focus on both reactor parameters (such as plasma power or discharge gap) and characteristics of the packing material (such as bead size, composition or presence of a catalyst) on CO_2 dissociation in DBD plasma aiming for a higher conversion and energy efficiency. Different packing materials have been investigated in CO_2 dissociation, such as SiO_2 [10, 11], Al_2O_3 [35], ZrO_2 [36], $BaTiO_3$ [37], quartz wool [34], ceramic foams [38], etc. As demonstrated in the above papers, the introduction of packing materials in the DBD reactor (often, but not always) enhances the CO_2 dissociation. Moreover, a combined effect of reactor parameters and packing materials' properties has been reported as well [31]. In these, it is postulated that synergistic effects between plasma and catalysts/packing material can enhance the conversion. However, this interaction between the plasma and material surface is still poorly understood [39].

The effect of the packing material properties, such as its crystalline phase, surface morphology or a composite composition, on CO_2 conversion did not gain significant attention. Introduction of a combination of oxides in the form of core-shells or the use of mixed metal oxides is nevertheless expected to influence the plasma properties at the packing material surface and

hence the conversion. In order to develop unambiguous insights into the effect of these factors, it is important to study the plasma process using packing materials with a systematically controlled structure and composition. Core-shell materials have been studied extensively in many applications because of the different chemical composition/combined effect on the surface and bulk [40]. However, there are only a few reports on core-shell structured materials in plasma catalysis [41-43]. To our knowledge, not many research has been reported on the influence of material properties on millimetre-sized core-shell spheres, as we investigated here. In addition, the properties of TiO_2 in plasma catalysis in the form of core-shell structures have not yet been explored. Here, a core-shell SiO_2@TiO_2 packing material has been introduced in a plasma-catalytic CO_2 dissociation in a DBD plasma reactor.

Titania (TiO_2) is a semiconductor material, widely investigated in many fields. It has a dielectric constant of 85-100, which can be the driving force to generate high energy electrons and localized dielectric discharges in plasma catalysis. In addition, Mei et al. also demonstrated the plasma-photocatalytic behaviour in TiO_2 and $BaTiO_3$ packing in CO_2 dissociation and reported a factor 2.5 enhancement of the conversion and energy efficiency in comparison to the reaction without the packing material [37]. It was suggested that the combined effect of semiconductor, photocatalytic and dielectric properties of TiO_2 might have an advantage in plasma-catalytic CO_2 dissociation [39]. Based on its semiconducting nature, its known oxygen vacancies and Ti^{3+}/Ti^{4+} transitions and surface charging, titania materials may have an interaction with the plasma species (radicals, ions, electrons or photons) that might influence conversion [39, 44]. Silica (SiO_2) is one of the most widely applied packing materials in packed bed DBD plasma reactors. Moreover, a combination of SiO_2 with titania (TiO_2) to form a composite material has been suitable for many catalytic processes, resulting in the enhancement of catalytic, structural and chemical properties [45]. Hence, TiO_2 is chosen as a shell layer for mm range core SiO_2 spheres as it might induce both physical (e.g. discharge, electric field enhancements) and chemical (surface) effects that influence plasma based CO_2 conversion.

TiO_2 has three main polymorphs namely anatase, rutile and brookite [46]. Of the three, anatase is one of the most widely studied crystal structure in many applications, like photocatalysis [47], heterogeneous thermal catalysis [48], photoelectrocatalysis [49], etc. Because of polymorphism, it is important to choose a suitable synthesis method for the coating process to achieve a core-shell SiO_2@TiO_2 with a controlled titania crystal phase. Requirements for the synthesis of the titania shell are that the precursor solution has good stability, the layer adheres well to the beads and the crystal structure is controlled and uniform. Several methods, such as sol-gel [50, 51],

hydrothermal [52], solvothermal [53] routes, etc., allow to successfully synthesize core-shell SiO_2@TiO_2 nanoparticles in a controlled way. However, in the DBD plasma reactor, the packing materials have dimensions in the mm range. As such large core spheres have a much stronger tendency to sediment, compared to nanosized core particles, the coating with a shell requires an adapted deposition approach, which has been developed in this work. When coating micrometer and millimeter sized materials, binders are often used to improve the homogeneous deposition on the packing materials. The contact surface between shell and core packing materials increases by the addition of binder, which improves adhesion. Mainly colloidal silica and alumina binders have been investigated depending on the application [54, 55]. Alumina has higher thermal stability than silica [55]. However, in this study, we opted for a binder with the same chemical composition as the support (core) because a different chemical composition could influence the packing material's physical and chemical properties towards the plasma, causing a strong influence on the catalytic performance.

Hence, a chemical solution based procedure was investigated to coat the mm range SiO_2 spheres with a TiO_2 layer by means of spray coating using stable water-based precursor solutions of citratoperoxotitanate(IV) complexes with and without the addition of a silica-based binder. We particularly focus on understanding the particular effect of the synthesis induced differences in the morphology of a TiO_2 shell, covering a SiO_2 core packing material, on the changes in plasma-catalytic CO_2 dissociation induced by the modified material properties such as surface morphology and loading of TiO_2.

2. Experimental Section

2.1. Chemicals required

The following chemicals were used for the preparation of the Ti(IV) precursor solution: titanium isopropoxide ($Ti(OC_3H_7)_4$, 98%, Acros), citric acid ($C_6H_8O_7$, 99.5%, Sigma-Aldrich), hydrogen peroxide (H_2O_2, 35 wt% in H_2O, Merck), ammonia (NH_3, 32% in H_2O, extra pure, Merck), non-porous SiO_2 spheres (1.6-1.8 mm, SiLibeads-type S, Sigmund Lindner) and LUDOX HS-40 colloidal silica as a binder (40 wt% suspension in H_2O, Merck).

2.2. Synthesis of aqueous citratoperoxotitanate(IV) precursor solution

An aqueous citratoperoxotitanate(IV) precursor solution was prepared following the reported route by Hardy et al. [56]. An appropriate volume of Ti(IV) isopropoxide (0.10 to 2.50 M) was added into an excess of H_2O. The white precipitate, formed as a result of hydrolysis and condensation, was collected via filtration and washed with water to remove byproducts. The

obtained wet white precipitate was then mixed with a solution of 3M citric acid (molar ratio of 1:1 against Ti^{4+}) and 35 wt% hydrogen peroxide (molar ratio of 1.5:1 against Ti^{4+}). This mixture was heated at 60˚C under constant stirring. After the precipitate dissolved, the solution's colour turned into dark red. Next, the pH of the dark red solution was adjusted to 7 by the dropwise addition of 32% ammonia. In this step, the dark red solution turned yellow-orange. The obtained solution was heated at 80˚C for 30 minutes. By the addition of water, different concentrations of citratoperoxotitanate(IV) precursor solutions ranging from 0.10 to 2.50 M were prepared.

To study the effect of adding a binder (LUDOX), three different concentrations of citratoperoxotitanate(IV) precursor (0.10, 0.25 and 0.50 M) solutions were prepared with and without LUDOX, respectively. In a 100 ml citratoperoxotitanate(IV) precursor solution, 0.1 wt% of LUDOX (against Ti^{4+}) was added and stirred for 1 hour.

Table 1: Experimental parameters of the precursor solutions used to prepare the core-shell spheres. The sample code SiO_2@TiO_2 – xM indicates that a precursor solution of x M Ti(IV) was used to spray coat around SiO_2 spheres. '+ LUDOX' is added to the sample code if a binder was mixed with the precursor solution prior to spray coating.

Sample code	**Concentration of citratoperoxotitanate(IV) precursor solution (M)**	**LUDOX[a] (wt% vs Ti^{4+})**
SiO_2	-	-
SiO_2@TiO_2 – 0.10M	0.10	-
SiO_2@TiO_2 – 0.25M	0.25	-
SiO_2@TiO_2 – 0.50M	0.50	-
SiO_2@TiO_2 – 0.10M+LUDOX	0.10	0.1
SiO_2@TiO_2 – 0.25M+LUDOX	0.25	0.1
SiO_2@TiO_2 – 0.50M+LUDOX	0.50	0.1
SiO_2@SiO_2 – 1.00M+LUDOX	1.00	0.1
SiO_2@TiO_2 – 1.50M+LUDOX	1.50	0.1
SiO_2@TiO_2 – 2.00M+LUDOX	2.00	0.1
SiO_2@TiO_2 – 2.50M+LUDOX	2.50	0.1

2.3. Spray Coating

The as-prepared citratoperoxotitanate(IV) precursor solutions with and without binder was spray coated onto SiO_2 spheres by means of a homebuilt drum spray coater [41]. The coated spheres dry during the spray coating process by a hot airflow. The coated SiO_2 core-shell spheres were then collected from the drum spray coater and calcined in a furnace at 650˚C for 4 hours in an ambient atmosphere, reached with a heating rate of 2˚C/min.

All prepared core-shell SiO_2@TiO_2 spheres were labelled as SiO_2@TiO_2 – xM (without LUDOX) and SiO_2@TiO_2 – xM+LUDOX (with LUDOX), where x is the concentration of the citratoperoxotitanate(IV) precursor solution (Table 1).

2.4. Plasma-Catalytic Experimental Setup

The experimental setup of the cylindrical packed-bed DBD reactor applied for plasma catalysis of CO_2 dissociation was discussed by Uytdenhouwen et al. [11]. A stainless steel rod with an outer diameter of 8 mm was used as the inner electrode. An alumina dielectric barrier was placed around the inner electrode. Its inner diameter was 17 mm, resulting in a discharge gap of 4.5 mm (between the inner electrode and the barrier). The outer diameter of the barrier was 21.8 mm, corresponding to a barrier thickness of 2.4 mm. A stainless-steel mesh with a length of 100 mm was wrapped around the dielectric tube to form the outer electrode. The inner electrode was grounded, while the outer electrode was powered by a high voltage, supplied by a generator (AFG 2021, Tektronix) and transformer (TREK, Model 20/20C-HS, x2000 voltage amplification). The applied voltage was measured with a high voltage probe (Tektronix P6015A), while a Rogowski coil (Pearson 4100) was used to measure the total current. Moreover, the voltage was measured on an external capacitor (10nF) to obtain the generated charges (Q) in the plasma. Finally, all electrical signals were recorded by an oscilloscope (Picotech, PicoScope 6402 D).

2.5. Space time measurements and extraction of kinetics data

The synthesized core-shell SiO_2@TiO_2 spheres (~ 23 ml) were packed in the entire discharge area with quartz wool at both ends of the reactor to hold the bed in place. Pure CO_2 gas was fed and controlled by a thermal mass flow controller. Plasma-catalytic CO_2 dissociation measurements of both packed and unpacked reactors were tested at a constant feed flow rate of 39 ml/min. While adding packing materials, the reactor volume decreased by 48.27% [31], so the feed flow was adjusted to 75 ml/min in the unpacked reactor to create a similar space time as the packed reactor with a feed flow rate of 39 ml/min (space time of 14.07 s). To study the

impact of the packing materials, the other experimental parameters, such as plasma power, frequency and discharge gap, were fixed at a constant value of 30 W, 3 kHz and 4.5 mm, respectively.

Moreover, the effect of the flow rate (space time) on the performance of the spherical core-shell packed reactor was evaluated by applying different feed flow rates, ranging from 8 to 219 ml/min (space time ranging from 2.5 to 70 s). More specifically, by tracking the reactor performance over a wide range of space times, key valuable kinetics data can be determined. Uytdenhouwen et al. developed an apparent first order reversible reaction to fit the experimental data and retrieve the equilibrium conversion and an overall reaction rate coefficient, as well as the individual CO_2 loss and formation rate coefficients, to quantify the reactor performance more fundamentally [31, 41, 57]. The equation (with derivation found in [57]) is defined as:

$$x_A\,(t) = x_{A,e} - (x_{A,e} - x_{A,i}\,)\;\; e^{-kt}, \quad (1)$$

where $x_{A,e}$ and $x_{A,i}$ are the equilibrium and initial mole fraction of A (with $x_{A,i} = 1$ for CO_2 dissociation), t is the space time and

$$k = f k_{\text{form}} + k_{\text{loss}} \quad (2)$$

$$x_{(A,e)} = \frac{f k_{\text{form}}}{f k_{\text{form}} + k_{\text{loss}}}. \quad (3)$$

k is the overall apparent rate coefficient with k_{loss} and $f\,k_{form}$ the apparent CO_2 loss and formation rate coefficients, respectively. The f factor is a constant that depends on the elemental composition of the system.

The equilibrium mole fraction $x_{A,e}$ can be rewritten in terms of the total equilibrium conversion X_e as:

$$X_e = \frac{k_{loss}}{f k_{\text{form}} + k_{\text{loss}}}. \quad (4)$$

The experimental data is fitted to equation (1) with MATLAB to retrieve k and x_e, and subsequently calculate the remaining values via equations (2) to (4).

2.6. Conversion and energy efficiency

The gas at the outlet of the reactor was analyzed by gas chromatography (GC) (Compact GC, Interscience). The GC is equipped with a thermal conductivity detector (TCD) and a flame

ionization detector, and 4 columns: a Molsieve 5A, 2 RT-Q bonds and an RTX-f column. The conversion of CO_2, X_{CO2}, from the GC data was determined by the following equation:

$$X_{CO_2} = \frac{CO_{2,in} - CO_{2,out}}{CO_{2,in}} \times 100\% \quad (5)$$

As one mole of CO_2 splits into 1 mole of CO and 0.5 mole of O_2, this gives a gas expansion factor of 1.5 for 100% conversion. As in the GC, the sample loop is depressurized to atmospheric pressure while injecting the reaction sample, some of the molecules are not detected when expansion of the gas has taken place. This causes an apparent lower peak area and CO_2 concentration and leads to an overestimation of CO_2 conversion. Therefore, the overestimated conversion has to be corrected, based on the actual gas conversion and expansion. The actual CO_2 conversion can be calculated by the following equation, defined by Pinhão et al. [58] and Snoeckx et al. [59].

$$X_{GC} = 1 - \left(\frac{1 - X_{CO_2}}{1 + \frac{X_{CO_2}}{2}}\right) \leftrightarrow X_{CO_2} = \frac{2X_{CO_2}}{3 - X_{GC}} \quad (6)$$

The energy efficiency of the conversion can be calculated via the following formula:

$$\eta\ (\%) = \frac{\Delta H_r \left(\frac{kJ}{mol}\right) * X_{CO_2}(\%)}{SEI\left(\frac{kJ}{L}\right) * 24.5\left(\frac{L}{mol}\right)} \quad (7)$$

Where ΔH_r is the reaction enthalpy of CO_2 dissociation (283 kJ/mol at 298.15 K), X_{CO_2} is the actual CO_2 conversion and a constant plasma power of 30 W is used to calculate the specific energy input (SEI) from the formula as follows

$$SEI\ \left(\frac{kJ}{L}\right) = \frac{Plasma\ Power\ (kW)}{Flow\ Rate\left(\frac{L}{min}\right)} * 60\ \left(\frac{s}{min}\right) \quad (8)$$

All the experiments were carried out with a freshly packed, cooled-down reactor and operated for a minimum amount of time of 40 min, to reach a thermal steady-state behaviour. The input voltage amplitude was continuously adjusted to the desired power of 30 W during the stabilization. Each experiment was tested in threefold for statistical review and for each experiment 4 GC measurements are taken, resulting in twelve data points per condition. The error bars were defined as:

$$error = \pm S_n \frac{T(p, n_s)}{\sqrt{n_s}} \quad (9)$$

With S_n the sample standard deviation of the measurements, n_s the sample size (12), and T the two-tailed inverse of the Student's t-distribution for sample size n_s and probability p set at 95%.

2.7. Chemical and physical characterization

Raman spectroscopy was performed with a Horiba Jobin Yvon T64000 triple Raman spectrometer, equipped with a BXFM Olympus microscope (10x magnification objective), a Horiba Jobin Yvon Symphony CCD detector and a 488 nm Lexel SHG laser operated at approximately 20 mW and with a spot size diameter of 2.381 µm. The confocal hole diameter was minimized to improve the spatial resolution. Raman spectroscopy recorded in all core-shell packing materials were measured at multiple spots of several spheres. The surface morphology of the (coated) packing spheres was characterized by using scanning electron microscopy (FEI Quanta 200FEG-SEM and Hitachi TM3000). SEM images were taken at multiple spots of several spheres.

3. Result and discussion

3.1. Titania crystal structure

The three main crystal structures of titania; namely anatase, rutile and brookite, can be identified by vibrational modes in Raman spectroscopy. Given the shape of the samples, it appeared difficult to collect the scattering from similar confocal volumes, and hence comparing intensities among the samples in not straightforward. All observed Raman modes (**Fig. 1(a)**) in SiO_2@TiO_2 – 0.10 M, 0.25 M and 0.50 M packing materials were in good agreement with the reported modes for anatase TiO_2. Anatase TiO_2 has six different Raman modes at 144 (E_g), 197 (E_g), 399 (B_{1g}), 516 (doublets of A_{1g} and B_{1g}) and 639 cm^{-1} (E_g), respectively [60]. The strongest E_g mode at 144 cm^{-1} assigned to external vibration of the anatase structure, is well resolved in all core-shell packing materials. This confirms the presence of TiO_2 around the SiO_2 spheres. It has been observed in SEM (§3.2) that the dense layer, formed at high concentration (0.5M) reveals poor adhesion with the core layer. It was observed that part of the TiO_2 layer detaches from the SiO_2 spheres, which could be due to stress occurring during heat treatment. The appearance of the SiO_2 Raman band at 1094 cm^{-1} **(Fig. S1)** in the SiO_2@TiO_2 – 0.50M packing material could therefore be an indication that the SiO_2 surface becomes more exposed due to detachment of the TiO_2 layer, which is further confirmed by SEM. The absence of a SiO_2 Raman band in the other two packing materials (SiO_2@TiO_2 – 0.10M and 0.25M) might point to a more continuous TiO_2 coverage of the SiO_2 surface.

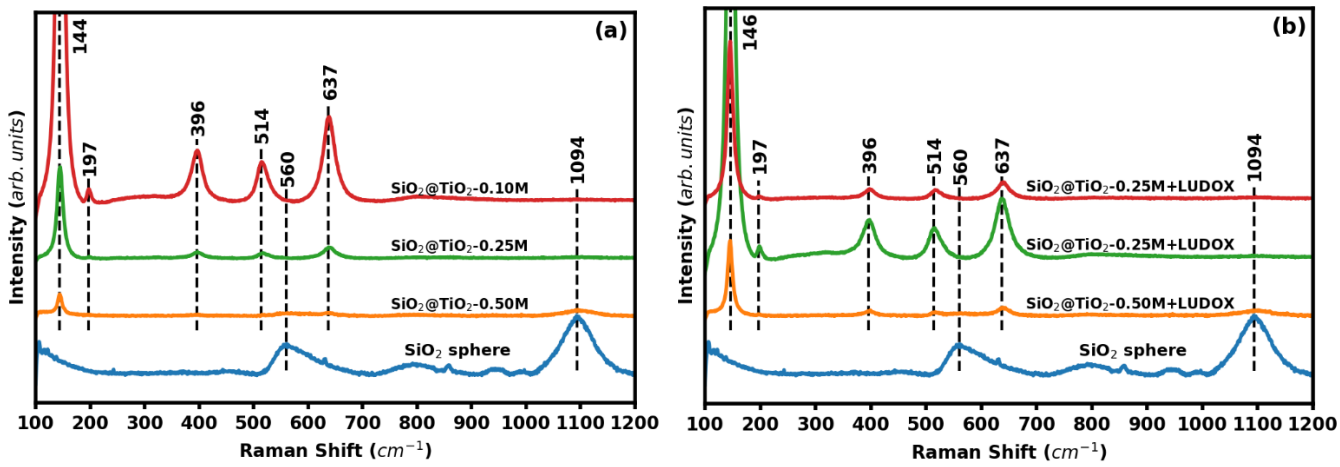

Figure 1. Raman spectra of core-shell spheres prepared with different concentrations of the Ti(IV) precursor solution (a) without a binder and (b) with a binder (LUDOX).

To study the role of the binder, Raman spectra for the packing materials were investigated, whereby LUDOX was added to the Ti(IV) precursor, which are shown in **Fig. 1(b).** For all the coated packing materials with LUDOX in the formulation, also the presence of anatase TiO_2 structure is demonstrated. There is no evidence of a phase transition of anatase to rutile for any of the coated spheres, even after heat treatment at 650˚C. Hence, we conclude that all the core-shell packing materials have a pure anatase TiO_2 crystal structure within the detection limit of the Raman spectrometer.

A SiO_2 Raman mode **(**magnification in **Fig. S1)** can be observed in the core-shell SiO_2@TiO_2 – 0.50M+LUDOX, which could originate from a higher local presence of silica in the sample resulting from the LUDOX or from SiO_2 constituting the core.

Also after plasma catalysis, the core-shell packing materials were characterized by Raman spectroscopy to inspect if the plasma reaction induces changes in the TiO_2 structure. The results **(Fig. S2)** confirm that the presence of anatase TiO_2 phase is retained even after plasma catalysis. In addition, surface defects such as oxygen vacancies or Ti vacancies can be investigated by Raman spectroscopy. The inset graph in **Fig. S2.** shows no shift or boarding of E_g mode (146 cm^{-1}) was observed, it confirms that there are no surface defects in the spent core-shell packing materials.

3.2. Surface Morphology

Surface morphology changes play an important role in catalysis, which can have either a positive or negative effect on the activity. More specifically, in case of plasma catalysis, cracks, edges,

and surface roughness could influence the plasma by changes in discharge behavior, local electric field enhancements, etc [39, 61]. To assess the effect of the concentration of the Ti(IV) precursor and the presence or absence of LUDOX in the coating formulation on the surface morphology of the TiO_2-coated silica spheres, packing materials coated with different concentrations of the citratoperoxotitanate(IV) precursor with and without LUDOX were characterized by scanning electron microscopy (SEM). **Fig. 2** shows the SEM images of bare SiO_2 spheres and SiO_2@TiO_2 – 0.10M spheres with and without LUDOX. A clear difference can be observed between uncoated and coated packing materials. The bare SiO_2 spheres have a smooth surface with some defects, whereas SiO_2@TiO_2 – 0.10M spheres with and without LUDOX show the deposition of a non-uniform coating consisting of TiO_2 islands. The TiO_2 structures have a higher backscatter yield compared to the SiO_2 surface and thus are brighter in the backscattered-electron (BSE) imaging mode. The non-uniformity might be due to an insufficient amount of TiO_2 to cover the SiO_2 surface, and/or by removal of organic compounds and crystallization during the heat treatment. However, it can be observed that the cracks formed on the coated SiO_2 surface are somewhat less in the samples with LUDOX compared to those without LUDOX. This illustrates that the addition of LUDOX increases the TiO_2 coverage of the SiO_2 spheres, even though the amount is not sufficient to form a continuous layer.

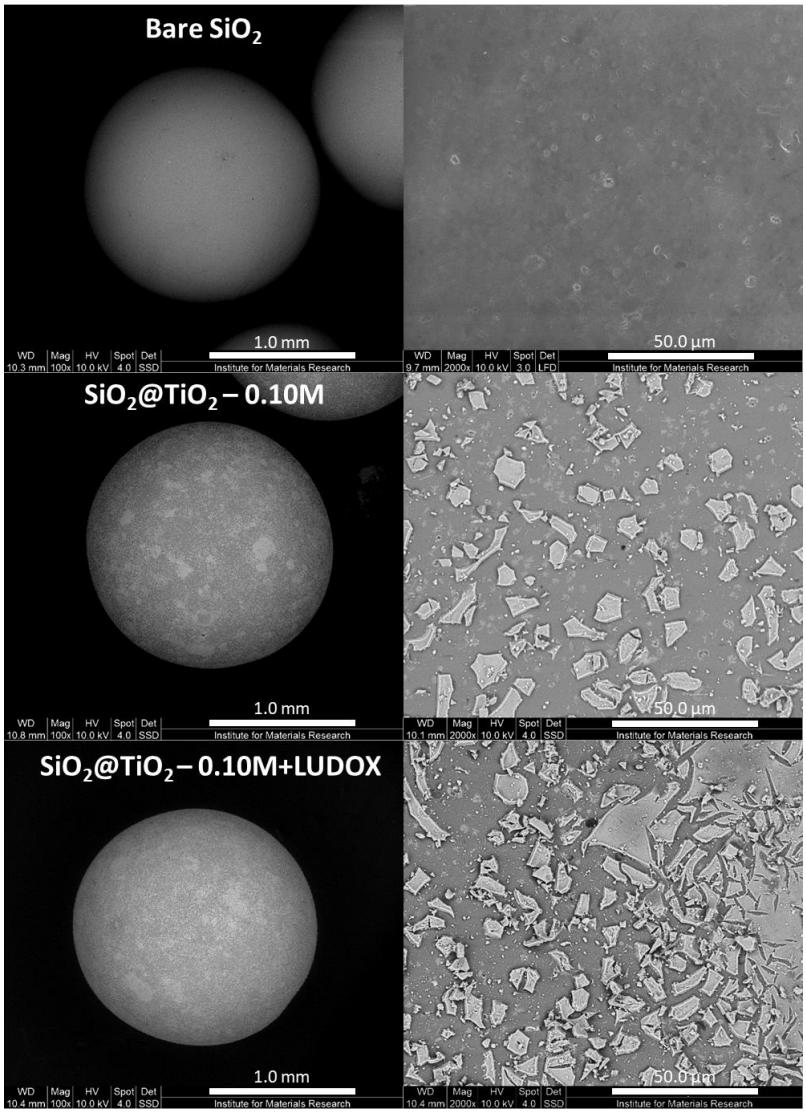

Figure 2. SEM images of bare SiO_2, core-shell $SiO_2@TiO_2$ – 0.10M spheres with and without LUDOX calcined at 650˚C.

The coverage of the TiO_2 layer was observed to improve when using higher concentrations of the titania precursor in $SiO_2@TiO_2$ – 0.25M spheres (without LUDOX). However, still cracks formed on the surface (**Fig. 3**). SEM images of $SiO_2@TiO_2$ – 0.25M packing materials **(Fig. S3)** confirm the formation of cracks even before calcination. Also, the formation of larger cracks due to evolution of gases during calcination can be observed. Nevertheless, further increase in Ti(IV) concentration to 0.50M in the core-shell particle without LUDOX does not provide better coating uniformity, as large flakes of TiO_2 are being formed on the surface (**Fig. 3**). After the calcination step of $SiO_2@TiO_2$ – 0.50M, TiO_2 powder was found to be deposited at the bottom of the sample container, indicating that part of the TiO_2 layer detaches and releases from the SiO_2 spherical particles at higher TiO_2 loading.

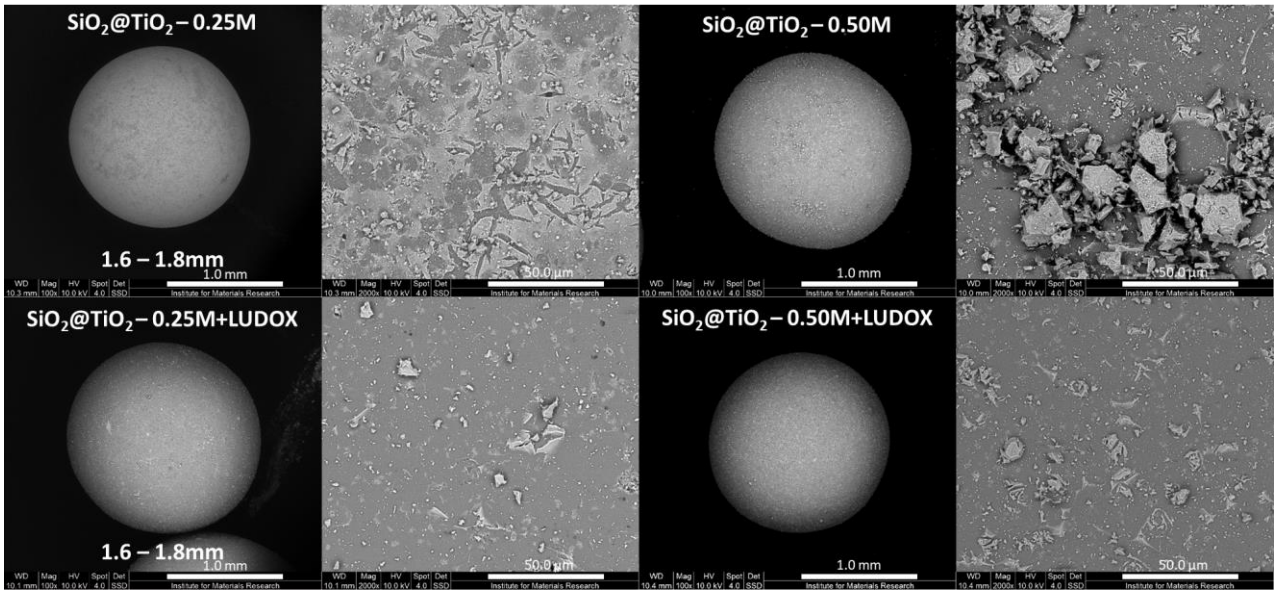

Figure 3. Surface morphology of core-shell SiO_2@TiO_2 – 0.25M and 0.50M spheres with and without LUDOX calcined at 650˚C.

The surface coverage improved in all core-shell SiO_2@TiO_2 spheres with LUDOX. In the SiO_2@TiO_2 – 0.25M+LUDOX and 0.5M+LUDOX spheres, the packing materials' surface appears more uniform with fewer cracks. Hence, the addition of LUDOX as a binder seems to improve the adhesion between core and shell layer [55]. SEM images **(Fig. 3)** of coated spheres with LUDOX confirm the improved adhesion between SiO_2 and TiO_2. However, the homogeneity of the coated layers varies on different SiO_2 spheres. Based on the results, it is clear that both the concentration of the titania precursor as well as the use of a binder material are important to obtain well controlled, crack free coated layers.

Surface morphology of core-shell packing materials has been evaluated after plasma catalysis experiments as well. The SEM images indicated that the surface morphology of the packing materials with LUDOX remained more or less the same as the original packing materials (**Fig. S4**), which suggests a sufficiently strong interaction between the SiO_2 and TiO_2 layer even after multipoint-space time measurements.

4. Plasma-catalytic measurement

4.1. Influence of TiO_2 loading

To study the influence of the TiO_2 loading on the plasma-assisted CO_2 conversion, the reaction was carried out by using different core-shell packing materials produced with concentrations of citratoperoxotitanate(IV) precursor solutions ranging from 0.10 M to 2.50 M containing LUDOX **(Fig. 4).** All experiments with different core-shell packing materials showed the same or a higher

CO_2 conversion and energy efficiency compared to the unpacked reactor or bare SiO_2 spheres as reference systems, irrespective of the flow rate. Although at a flow rate of 39 ml/min (similar to the packed reactor), the positive effect of the packing on the conversion is present, in most cases it is relatively small (in the range of 4-5% more conversion) taken into account the error bars (1-2%). Nevertheless, it demonstrates that the introduction of a dielectric material (TiO_2) as a shell layer on SiO_2 spheres is able to enhance the conversion, as also indicated in literature [37]. When the concentration of the Ti(IV) solution increases from 0.10 M to 0.25 M, the CO_2 conversion increases by 4%. However, a further increase in the concentration to 0.50 M leads to a decrease in conversion by 3%. The conversion and energy efficiency remain more or less constant when increasing the concentration further from 0.50 M to 2.50 M. Based on the data of conversion and the morphological characteristics described before, this confirms that core-shell spheres prepared with a low concentration of Ti(IV) precursor solutions (as is the case for 0.25 M and 0.50 M) might be more beneficial. A further increase in the concentration results in TiO_2 layers that peeled off from the SiO_2 spheres, which causes more exposed SiO_2 surface and surface roughness with edges and SiO_2/TiO_2 contacts and is likely responsible for the lower conversion. When compared with the unpacked reactor at the same space time, the conversion is significantly higher for core-shell packing materials with lower concentration of Ti(IV) precursor solutions. Also, the energy efficiency of the core-shell packing materials are much higher than the unpacked reactor. Here the increase is much larger when compared at same flow rate, but even at same space time, the energy efficiency is higher (in spite of the higher SEI). Hence, SiO_2@TiO_2 – 0.10M, 0.25M and 0.50M spheres (with LUDOX) were chosen as optimized packing materials for further measurements.

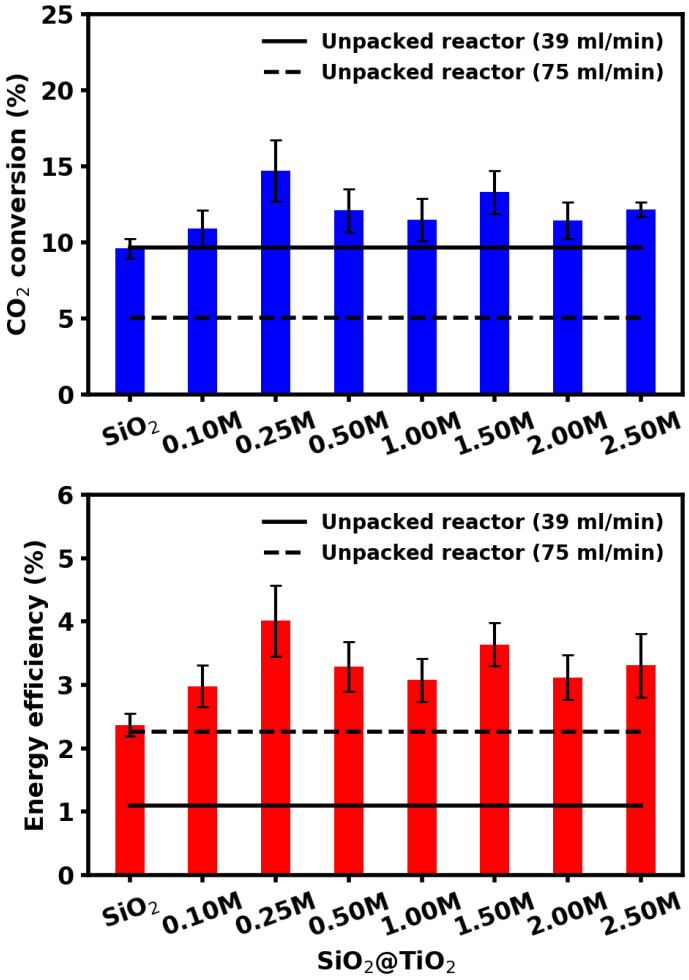

Figure 4. Plasma-catalytic CO_2 conversion and corresponding energy efficiency, in function of the different concentrations of Ti(IV) precursor solutions with LUDOX coated on SiO_2 spheres, compared to the unpacked reactor at the same flow rate (39 ml/min) and at the same space time (14.07 s; flow rate of 75 ml/min).

4.2. Impact of LUDOX as a binder

As observed from Raman spectra and SEM images, a binder (LUDOX) was used to improve the uniformity of the TiO_2 shell layer. The effect of the binder on the conversion and energy efficiency was studied by comparing the CO_2 conversion using core-shell spheres with and without LUDOX in the DBD reactor. All the measurements were performed at 14.07 s space time, where the conversion results show a significant difference in the packing material with and without LUDOX **(Fig. 5)**. The highest CO_2 conversion and energy efficiency of 15% and 4%, respectively, were obtained for SiO_2@TiO_2 – 0.25M with LUDOX, being the packing material that shows the most continuous shell of TiO_2 around the SiO_2 spheres. It can be deduced that it is important to have a continuous layer of dielectric material covering the SiO_2 packing material. The enhanced

performance can be ascribed to different aspects which cannot be distinguished, such as the possibility to produce high energy electrons at the contact point of two spheres [62] or the generation of highly active (charged) sites at the surface or differences in discharge mode [39, 63]. Other possible unidentified material effects cannot be excluded at this point. This concurs with the conclusion of Mei et al. who indicated synergy when using titania pellets in the plasma discharge for CO_2 conversion (conversion improved by a factor of 2.5) and attributed this to a combination of physical and chemical effects, including those induced at the photocatalytic surface driven by high energy electrons from the CO_2 discharge rather than the photons in the plasma [37].

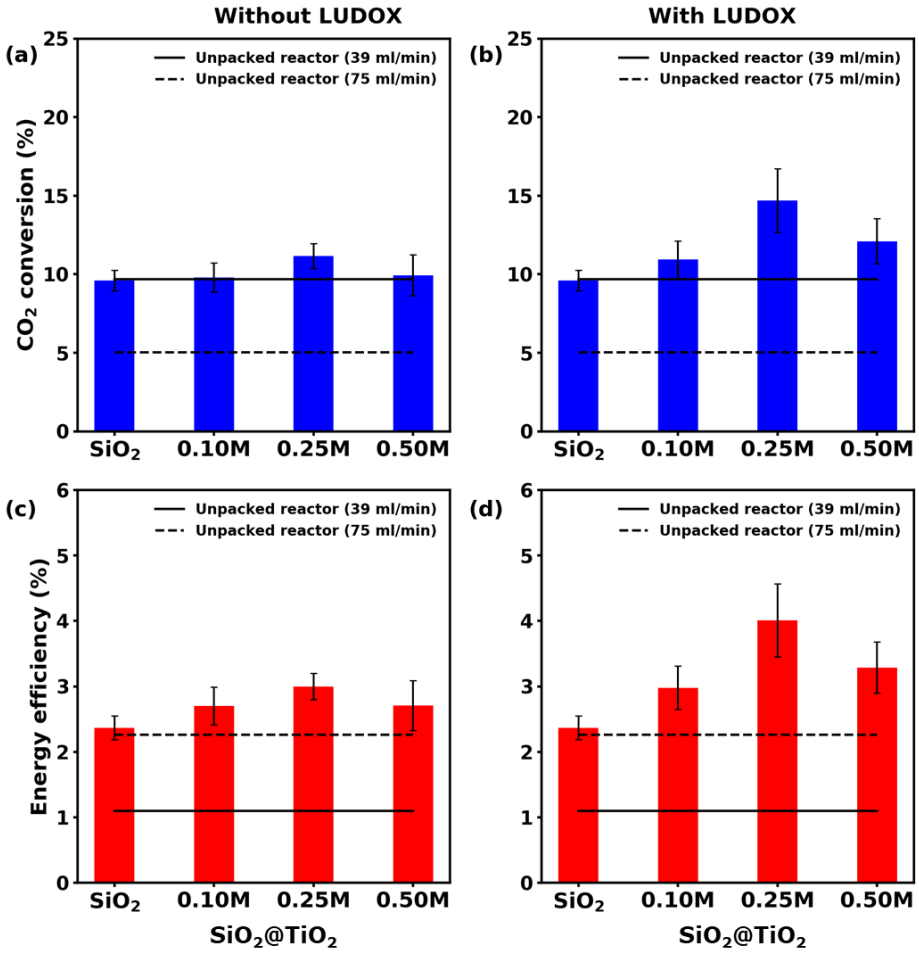

Figure 5. Plasma-catalytic activity on core-shell $SiO_2@TiO_2$ spheres without LUDOX (a & c) and with LUDOX (b & d) in function of the applied concentration of Ti(IV) precursor during coating of the SiO_2 core material, compared to the unpacked reactor at same flow rate (39 ml/min) and at same space time (14.07 s; flow rate of 75 ml/min).

If the spheres have cracks or a non-continuous layer of TiO_2, there is more possibility for contact points between SiO_2 and TiO_2 or SiO_2 and SiO_2, which might reduce the number of high energy electrons, which might cause the lower increase in conversion [64].

4.3. Effect of space time

The single point measurements presented here, showed an approximate idea of activity at short space time, which is not an ideal condition to make any conclusion on conversion or performance. Therefore, the recommendation towards multipoint-space time measurements for plasma-catalytic reactions, made in previous work and demonstrated on uncoated dense spheres, was followed [11, 31, 57]. Hence, to validate the conversion results at steady-state conditions, the changes in the conversion with respect to space time for CO_2 dissociation were evaluated at space times ranging from 2.5 to 70 s for an unpacked reactor and a reactor with a packing of SiO_2, SiO_2@TiO_2 – 0.10M+LUDOX and SiO_2@TiO_2 – 0.25M+LUDOX **(Fig. 6).** A constant volume of the catalyst was used in CO_2 conversion; hence the results presented as a function of space time is also represented in GHSV **(Fig. S5.)**.

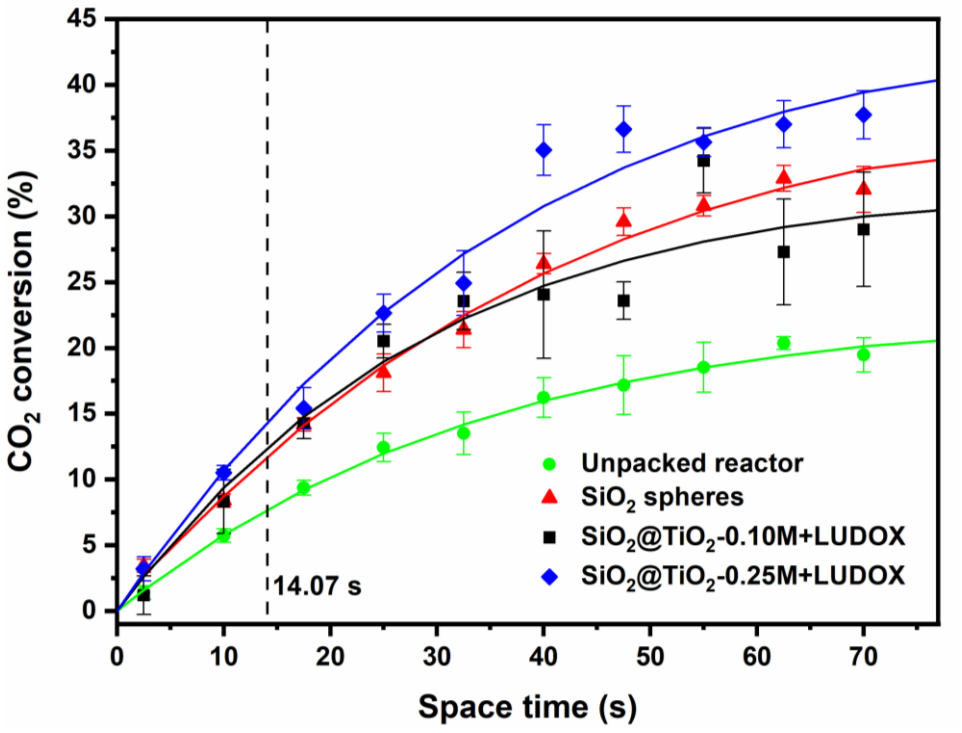

Figure 6. Plasma-catalytic CO_2 conversion as a function of space time; compared with single-point space time (vertical dashed line).

Increasing the flow rate will reduce the conversion because of the shorter space time and thus contact with the plasma and the packing material. However, with decreasing flow rate, and thus

increasing space time, the conversion increases until a certain point and then becomes more constant for all packed and unpacked reactors. It is clear that with increasing space time, the impact of the different packing materials becomes more pronounced, as was also observed for other packing materials [31]. The space time measurement confirms that the packing material enhances the conversion of CO_2, proving the packing effect in the plasma reaction.

Table 2: Fitted kinetic and partial chemical equilibrium data for the CO_2 splitting reaction, at a plasma power of 30 W and a frequency of 3 kHz, in a 4.5 mm gap size reactor.

samples	k (s^{-1})	X_e (%)	k_{loss} (s^{-1})	f k_{form} (s^{-1})
Unpacked reactor	0.032 ± 0.005	23 ± 2	0.007 ± 0.002	0.025 ± 0.006
SiO_2 spheres	0.027 ± 0.002	40 ± 2	0.011 ± 0.001	0.016 ± 0.002
SiO_2@TiO_2 – 0.10M+LUDOX	0.039 ± 0.009	33 ± 3	0.013 ± 0.004	0.026 ± 0.009
SiO_2@TiO_2 – 0.25M+LUDOX	0.032 ± 0.004	45 ± 3	0.015 ± 0.003	0.018 ± 0.003

A comparison was made for the activity of core-shell SiO_2@TiO_2 – 0.10M+LUDOX and 0.25M+LUDOX materials based on the multiple-point measurement. Even though the SiO_2@TiO_2 – 0.10M+LUDOX packing material exhibited a slightly better conversion at the single point measurement (14.07 s space time), it converted less CO_2 than the packing consisting of bare SiO_2 spheres at longer space times where partial chemical equilibrium is being reached. This suggests that the formation of cracks and exposed SiO_2 surface in the core-shell packing material have a negative effect on the CO_2 dissociation, which could confirm the indicated reduced number of high energy electrons as predicted by simulations [64]. Nevertheless, we cannot exclude other possible occurring mechanisms that might be responsible for the inferior partial chemical equilibrium conversion such as, but not limited to, e.g. diffusion limitations in the coated layer, material boundary and edge effects that influence the discharge, the electric field etc. Moreover, the continuous layer of TiO_2 with less apparent cracks (SiO_2@TiO_2 – 0.25M+LUDOX) showed the highest CO_2 conversion and energy efficiency **(Fig. S6.)** of 37.7% and 1.8 % at 70 s respectively at the conditions applied here. The highest CO_2 conversion, obtained for SiO_2 and SiO_2@TiO_2 – 0.10M+LUDOX spheres was 32% and 29% at 70 s, respectively. However, the highest energy efficiency of 4.8% was achieved at 2.5 s for SiO_2@TiO_2 – 0.25M+LUDOX spheres. At this space time, SiO_2 spheres and SiO_2@TiO_2 – 0.10M+LUDOX showed energy efficiencies of 4.4% and 1.8 %, although all with a large error on the measurement. The kinetic and partial chemical equilibrium of the CO_2 dissociation using

unpacked and packed reactors are shown in **Table 2**. The fitted reaction coefficient for the CO_2 loss reactions (k_{loss}) increases with a factor of 1.5 from empty to SiO_2 spheres, while the fitted reaction coefficient for the formation of CO_2 reactions (f k_{form}) decreases with a factor of 1.5. This is the reason that overall the global rate coefficient (k) stays about the same while the equilibrium is shifted away from CO_2 due to more loss and less formation. Similarly, coating with 0.10 M TiO_2 further increases the loss rate coefficient but apparently also increases the formation term from 0.016 s^{-1} to 0.026 s^{-1}; perhaps due to some surface effect from the inhomogeneous, cracked TiO_2 layer, possibly promoting the reaction of CO and O_2 back into CO_2. It caused a decrease in the equilibrium conversion (X_e) to 33% and increase in the global rate coefficient to 0.039 s^{-1}. That is also the reason why the single-point space time measurements of SiO_2@TiO_2 – 0.10M+LUDOX seemed better than those of SiO_2 - because of the higher reaction rate coefficient. However, in these multipoint space time measurements the SiO_2@TiO_2 – 0.10M+LUDOX sample performs worse than SiO_2 because the equilibrium conversion is lower. Lastly, adding more TiO_2 (SiO_2@TiO_2 – 0.25M+LUDOX) apparently further increases the loss reaction rate to 0.015 s^{-1} and lowers the formation rate to 0.018 s^{-1}. It shows that an increase in the TiO_2 loading and coverage of TiO_2 layer with less apparent cracks, improves CO_2 splitting and reduces the CO_2 formation reactions. From the multipoint space time measurements, it can therefore be deduced that the introduction of packing materials in the form of core-shell structure as well as the morphology, loading and presence of binders of the coated shell, have a huge impact on the plasma-assisted CO_2 conversion, due to the combination of physical and chemical, surface and bulk properties. Although the data clearly show that these effects change the apparent partial chemical equilibrium (X_e) proving a physical and/or chemical effect of the packing material on the conversion process, there is no clear evidence of a catalytic effect. For, although the rate coefficient of SiO_2@TiO_2-0.10M+LUDOX seems enhanced, the difference not significant. Moreover, the rate of the loss and formation reaction is not influenced in the same way. Hence, it is difficult to conclude whether a true catalytic effect is present on top of the clear physical/chemical effect.

5. Conclusion:

Core-shell SiO_2@TiO_2 spheres with and without LUDOX were successfully prepared by spray coating aqueous citratoperoxotitanate(IV) precursor solutions at different concentrations, followed by thermal processing. The obtained TiO_2 coatings were shown to exhibit an anatase crystal structure in Raman spectroscopy. From SEM, it was confirmed that at a too high concentration (0.50 M), the TiO_2 partly detaches from the sphere and more cracks and island-

like TiO_2 coatings are being formed. Using 0.1 wt% LUDOX as a binder improves the layer's continuity and reduces cracks and formation of separate TiO_2 island-like structures. Plasma-assisted CO_2 dissociation experiments confirm the impact of surface changes, induced by the preparation condition of the shell and the morphology of the core-shell layer. The maximum CO_2 conversion of 37.7% (at a residence time of 70 s corresponding to an energy efficiency of 2%) and the highest energy efficiency of 4.8% (at a residence time of 2.5 s corresponding to a conversion of 3%) are obtained with SiO_2@TiO_2 – 0.25M spheres with LUDOX at 30 W, 3 kHz and a 4.5 mm discharge gap. These results confirm that core-shell spheres are promising packing materials to enhance the plasma performance compared to bare SiO_2 spheres and unpacked reactors, when the properties of the shell can be sufficiently controlled. Here, we have adopted a solution-based method to coat mm range spheres and investigated the changes in surface morphology and TiO_2 loading on the core-shell packing materials and their effect in the plasma-catalytic CO_2 conversion. It is clear that materials have a high potential in plasma-based conversion processes, while the impact of material properties on conversion needs more detailed attention.

CRediT authorship contribution statement

Periyasamy Kaliyappan: Writing – Original draft preparation, Data curation, Investigation, Conceptualization **Andreas Paulus:** Investigation **Jan D'Haen:** Investigation **Pieter Samyn:** Resource, Writing – review & editing **Yannick Uytdenhouwen:** Formal analysis, methodology **Neda Hafezkhiabani:** Methodology **Annemie Bogaerts:** writing – review & editing **Vera Meynen:** Writing – review & editing, Conceptualization **Ken Elen:** Writing – review & editing **An Hardy:** Supervision, Writing – review & editing, Conceptualization **Marlies K. Van Bael:** Supervision, Writing – review & editing, Conceptualization

Declaration of competing interest

The authors declare that they have no known competing financial interests or personal relationships that could have appeared to influence the work reported in this paper.

Acknowledgement

We acknowledge financial support from the European Fund for Regional Development through the cross-border collaborative Interreg V program Flanders-the Netherlands [project EnOp] with co-financing from the Belgian province of Limburg, the Fund for Scientific Research [FWO; Grant Number: G.0254014N], an IOF-SBO [SynCO2Chem] project and PlasmaCatDesign [FWO-SBO; Grant Number: S001619N] project. We would also like to thank Jasper Lefevere from

VITO [Vlaamse Instelling voor Technologisch Onderzoek – Flemish institute for technology research] for providing a protocol for LUDOX as a binder and Karen Leyssens and Saskia Defossé from Universiteit Antwerp [Laboratory of Adsorption & Catalysis (LADCA), Department of Chemistry, University of Antwerp] for the plasma-catalytic measurements.

Appendix A. Supplementary data

The following is Supplementary data to this article

References

[1] M.S.G. Lopes, Renewable and Advanced Materials as a Powerful Tool to Mitigate Climate Change, World News-Climate Change The New Economy Ltd, G 7 Climate Change The New Economy, 2018.
[2] X. Xiaoding, J.A. Moulijn, Mitigation of CO_2 by Chemical Conversion: Plausible Chemical Reactions and Promising Products, Energy & Fuels 10(2) (1996) 305-325.
[3] N. MacDowell, N. Florin, A. Buchard, J. Hallett, A. Galindo, G. Jackson, C.S. Adjiman, C.K. Williams, N. Shah, P. Fennell, An overview of CO_2 capture technologies, Energy & Environmental Science 3(11) (2010) 1645-1669.
[4] C. Song, Global challenges and strategies for control, conversion and utilization of CO_2 for sustainable development involving energy, catalysis, adsorption and chemical processing, Catalysis Today 115(1) (2006) 2-32.
[5] G. Centi, S. Perathoner, Opportunities and prospects in the chemical recycling of carbon dioxide to fuels, Catalysis Today 148(3) (2009) 191-205.
[6] E.A. Quadrelli, G. Centi, J.L. Duplan, S. Perathoner, Carbon dioxide recycling: emerging large-scale technologies with industrial potential, ChemSusChem 4(9) (2011) 1194-215.
[7] J. Guo, H. Lou, H. Zhao, D. Chai, X. Zheng, Dry reforming of methane over nickel catalysts supported on magnesium aluminate spinels, Applied Catalysis A: General 273(1) (2004) 75-82.
[8] X. Tu, J.C. Whitehead, Plasma-catalytic dry reforming of methane in an atmospheric dielectric barrier discharge: Understanding the synergistic effect at low temperature, Applied Catalysis B: Environmental 125 (2012) 439-448.
[9] X. Tu, H.J. Gallon, M.V. Twigg, P.A. Gorry, J.C. Whitehead, Dry reforming of methane over a Ni/Al_2O_3catalyst in a coaxial dielectric barrier discharge reactor, Journal of Physics D: Applied Physics 44(27) (2011) 274007.
[10] I. Michielsen, Y. Uytdenhouwen, J. Pype, B. Michielsen, J. Mertens, F. Reniers, V. Meynen, A. Bogaerts, CO_2 dissociation in a packed bed DBD reactor: First steps towards a better understanding of plasma catalysis, Chemical Engineering Journal 326 (2017) 477-488.
[11] Y. Uytdenhouwen, S. Van Alphen, I. Michielsen, V. Meynen, P. Cool, A. Bogaerts, A packed-bed DBD micro plasma reactor for CO_2 dissociation: Does size matter?, Chemical Engineering Journal 348 (2018) 557-568.
[12] L. Wang, Y. Yi, H. Guo, X. Tu, Atmospheric Pressure and Room Temperature Synthesis of Methanol through Plasma-Catalytic Hydrogenation of CO_2, ACS Catalysis 8(1) (2018) 90-100.
[13] S.C. Roy, O.K. Varghese, M. Paulose, C.A. Grimes, Toward Solar Fuels: Photocatalytic Conversion of Carbon Dioxide to Hydrocarbons, ACS Nano 4(3) (2010) 1259-1278.
[14] K. Zhang, B. Eliasson, U. Kogelschatz, Direct Conversion of Greenhouse Gases to Synthesis Gas and C_4 Hydrocarbons over Zeolite HY Promoted by a Dielectric-Barrier Discharge, Industrial & Engineering Chemistry Research 41(6) (2002) 1462-1468.
[15] A. Gómez-Ramírez, V.J. Rico, J. Cotrino, A.R. González-Elipe, R.M. Lambert, Low Temperature Production of Formaldehyde from Carbon Dioxide and Ethane by Plasma-Assisted Catalysis in a

Ferroelectrically Moderated Dielectric Barrier Discharge Reactor, ACS Catalysis 4(2) (2014) 402-408.
[16] S.S. Kim, S.M. Lee, S.C. Hong, A study on the reaction characteristics of CO_2 decomposition using iron oxides, Journal of Industrial and Engineering Chemistry 18(2) (2012) 860-864.
[17] W. Keim, Carbon monoxide: feestock for chemicals, present and future, Journal of Organometallic Chemistry 372(1) (1989) 15-23.
[18] D.D. Wagman, J.E. Kilpatrick, W.J. Taylor, K.S. Pitzer, F.D. Rossini, Heats, free energies, and equilibrium constants of some reactions involving O_2, H_2, H_2O, C, CO, CO_2, and CH_4, Journal of Research of the National Bureau of Standards 34(2) (1945) 143.
[19] S. Rayne, Thermal Carbon Dioxide Splitting: A Summary of the Peer-Reviewed Scientific Literature, Nature Precedings (2008).
[20] D. Mei, X. Zhu, Y.-L. He, J.D. Yan, X. Tu, Plasma-assisted conversion of CO_2 in a dielectric barrier discharge reactor: understanding the effect of packing materials, Plasma Sources Science and Technology 24(1) (2014) 015011.
[21] R. Snoeckx, A. Bogaerts, Plasma technology – a novel solution for CO_2 conversion?, Chemical Society Reviews 46(19) (2017) 5805-5863.
[22] U. Kogelschatz, Applications of Microplasmas and Microreactor Technology, 47(1-2) (2007) 80-88.
[23] T. Silva, N. Britun, T. Godfroid, R. Snyders, Optical characterization of a microwave pulsed discharge used for dissociation of CO_2, Plasma Sources Science and Technology 23(2) (2014) 025009.
[24] S. Heijkers, R. Snoeckx, T. Kozák, T. Silva, T. Godfroid, N. Britun, R. Snyders, A. Bogaerts, CO_2 Conversion in a Microwave Plasma Reactor in the Presence of N_2: Elucidating the Role of Vibrational Levels, The Journal of Physical Chemistry C 119(23) (2015) 12815-12828.
[25] L.F. Spencer, A.D. Gallimore, CO_2 dissociation in an atmospheric pressure plasma/catalyst system: a study of efficiency, Plasma Sources Science and Technology 22(1) (2012) 015019.
[26] A. Indarto, D.R. Yang, J.-W. Choi, H. Lee, H.K. Song, Gliding arc plasma processing of CO_2 conversion, Journal of Hazardous Materials 146(1) (2007) 309-315.
[27] T. Nunnally, K. Gutsol, A. Rabinovich, A. Fridman, A. Gutsol, A. Kemoun, Dissociation of CO_2 in a low current gliding arc plasmatron, Journal of Physics D: Applied Physics 44(27) (2011) 274009.
[28] S. Heijkers, A. Bogaerts, CO_2 Conversion in a Gliding Arc Plasmatron: Elucidating the Chemistry through Kinetic Modeling, The Journal of Physical Chemistry C 121(41) (2017) 22644-22655.
[29] R. Aerts, W. Somers, A. Bogaerts, Carbon Dioxide Splitting in a Dielectric Barrier Discharge Plasma: A Combined Experimental and Computational Study, 8(4) (2015) 702-716.
[30] M. Ramakers, I. Michielsen, R. Aerts, V. Meynen, A. Bogaerts, Effect of Argon or Helium on the CO_2 Conversion in a Dielectric Barrier Discharge, Plasma Processes and Polymers 12(8) (2015) 755-763.
[31] Y. Uytdenhouwen, K.M. Bal, I. Michielsen, E.C. Neyts, V. Meynen, P. Cool, A. Bogaerts, How process parameters and packing materials tune chemical equilibrium and kinetics in plasma-based CO_2 conversion, Chemical Engineering Journal 372 (2019) 1253-1264.
[32] K. Zhang, G. Zhang, X. Liu, A.N. Phan, K. Luo, A Study on CO_2 Decomposition to CO and O_2 by the Combination of Catalysis and Dielectric-Barrier Discharges at Low Temperatures and Ambient Pressure, Industrial & Engineering Chemistry Research 56(12) (2017) 3204-3216.
[33] U. Kogelschatz, Dielectric-Barrier Discharges: Their History, Discharge Physics, and Industrial Applications, Plasma Chemistry and Plasma Processing 23(1) (2003) 1-46.
[34] X. Duan, Z. Hu, Y. Li, B. Wang, Effect of dielectric packing materials on the decomposition of carbon dioxide using DBD microplasma reactor, 61(3) (2015) 898-903.
[35] Q. Yu, M. Kong, T. Liu, J. Fei, X. Zheng, Characteristics of the Decomposition of CO_2 in a Dielectric Packed-Bed Plasma Reactor, Plasma Chemistry and Plasma Processing 32(1) (2012) 153-163.
[36] A. Zhou, D. Chen, C. Ma, F. Yu, B. Dai, DBD Plasma-ZrO_2 Catalytic Decomposition of CO_2 at Low Temperatures, Catalysts 8(7) (2018) 256.

[37] D. Mei, X. Zhu, C. Wu, B. Ashford, P.T. Williams, X. Tu, Plasma-photocatalytic conversion of CO_2 at low temperatures: Understanding the synergistic effect of plasma-catalysis, Applied Catalysis B: Environmental 182 (2016) 525-532.
[38] Y.-f. Guo, D.-q. Ye, K.-f. Chen, J.-c. He, Toluene removal by a DBD-type plasma combined with metal oxides catalysts supported by nickel foam, Catalysis Today 126(3) (2007) 328-337.
[39] A. Bogaerts, X. Tu, J.C. Whitehead, G. Centi, L. Lefferts, O. Guaitella, F. Azzolina-Jury, H.-H. Kim, A.B. Murphy, W.F. Schneider, T. Nozaki, J.C. Hicks, A. Rousseau, F. Thevenet, A. Khacef, M. Carreon, The 2020 plasma catalysis roadmap, Journal of Physics D: Applied Physics 53(44) (2020) 443001.
[40] S. Das, J. Pérez-Ramírez, J. Gong, N. Dewangan, K. Hidajat, B.C. Gates, S. Kawi, Core–shell structured catalysts for thermocatalytic, photocatalytic, and electrocatalytic conversion of CO_2, Chemical Society Reviews 49(10) (2020) 2937-3004.
[41] Y. Uytdenhouwen, V. Meynen, P. Cool, A. Bogaerts, The Potential Use of Core-Shell Structured Spheres in a Packed-Bed DBD Plasma Reactor for CO_2 Conversion, Catalysts 10(5) (2020) 530.
[42] X. Zheng, S. Tan, L. Dong, S. Li, H. Chen, $LaNiO_3$@SiO_2 core–shell nano-particles for the dry reforming of CH_4 in the dielectric barrier discharge plasma, International Journal of Hydrogen Energy 39(22) (2014) 11360-11367.
[43] X. Zheng, S. Tan, L. Dong, S. Li, H. Chen, Plasma-assisted catalytic dry reforming of methane: Highly catalytic performance of nickel ferrite nanoparticles embedded in silica, Journal of Power Sources 274 (2015) 286-294.
[44] A. Jafarzadeh, K.M. Bal, A. Bogaerts, E.C. Neyts, CO_2 Activation on TiO_2-Supported Cu_5 and Ni_5 Nanoclusters: Effect of Plasma-Induced Surface Charging, The Journal of Physical Chemistry C 123(11) (2019) 6516-6525.
[45] X. Gao, I.E. Wachs, Titania–silica as catalysts: molecular structural characteristics and physico-chemical properties, Catalysis Today 51(2) (1999) 233-254.
[46] X. Chen, S.S. Mao, Titanium Dioxide Nanomaterials: Synthesis, Properties, Modifications, and Applications, Chemical Reviews 107(7) (2007) 2891-2959.
[47] T. Luttrell, S. Halpegamage, J. Tao, A. Kramer, E. Sutter, M. Batzill, Why is anatase a better photocatalyst than rutile? - Model studies on epitaxial TiO_2 films, Scientific Reports 4(1) (2014) 4043.
[48] S. Huygh, A. Bogaerts, E.C. Neyts, How Oxygen Vacancies Activate CO_2 Dissociation on TiO_2 Anatase (001), The Journal of Physical Chemistry C 120(38) (2016) 21659-21669.
[49] H. Zhang, Y. Wang, P. Liu, Y. Han, X. Yao, J. Zou, H. Cheng, H. Zhao, Anatase TiO_2 Crystal Facet Growth: Mechanistic Role of Hydrofluoric Acid and Photoelectrocatalytic Activity, ACS Applied Materials & Interfaces 3(7) (2011) 2472-2478.
[50] J.-W. Lee, S. Kong, W.-S. Kim, J. Kim, Preparation and characterization of SiO_2/TiO_2 core-shell particles with controlled shell thickness, Materials Chemistry and Physics 106(1) (2007) 39-44.
[51] L. Wu, Y. Zhou, W. Nie, L. Song, P. Chen, Synthesis of highly monodispersed teardrop-shaped core–shell SiO_2/TiO_2 nanoparticles and their photocatalytic activities, Applied Surface Science 351 (2015) 320-326.
[52] S. Ullah, E.P. Ferreira-Neto, A.A. Pasa, C.C.J. Alcântara, J.J.S. Acuña, S.A. Bilmes, M.L. Martínez Ricci, R. Landers, T.Z. Fermino, U.P. Rodrigues-Filho, Enhanced photocatalytic properties of core@shell SiO_2@TiO_2 nanoparticles, Applied Catalysis B: Environmental 179 (2015) 333-343.
[53] H. Zhang, G. Wang, G. Sun, F. Xu, H. Li, S. Li, S. Fu, Facile synthesis of SiO_2@TiO_2 hybrid NPs with improved photocatalytic performance, Micro & Nano Letters 13(5) (2018) 666-668.
[54] X. Kong, M. Qiu, A. Wang, L. Yang, R. Zhou, Y. Fan, D. Kong, C. Gu, Influence of alumina binders on adhesion and cohesion during preparation of Cu-SAPO-34/monolith catalysts, International Journal of Applied Ceramic Technology 15(6) (2018) 1490-1501.
[55] C.P. Rodrigues, E. Kraleva, H. Ehrich, F.B. Noronha, Structured Reactors as an Alternative to Fixed-bed Reactors: Influence of catalyst preparation methodology on the partial oxidation of ethanol, Catalysis Today 273 (2016) 12-24.

[56] A. Hardy, J. D'Haen, M.K. Van Bael, J. Mullens, An aqueous solution–gel citratoperoxo–Ti(IV) precursor: synthesis, gelation, thermo-oxidative decomposition and oxide crystallization, Journal of Sol-Gel Science and Technology 44(1) (2007) 65-74.
[57] Y. Uytdenhouwen, K.M. Bal, E.C. Neyts, V. Meynen, P. Cool, A. Bogaerts, On the kinetics and equilibria of plasma-based dry reforming of methane, Chemical Engineering Journal (2020) 126630.
[58] N. Pinhão, A. Moura, J.B. Branco, J. Neves, Influence of gas expansion on process parameters in non-thermal plasma plug-flow reactors: A study applied to dry reforming of methane, International Journal of Hydrogen Energy 41(22) (2016) 9245-9255.
[59] R. Snoeckx, S. Heijkers, K. Van Wesenbeeck, S. Lenaerts, A. Bogaerts, CO_2 conversion in a dielectric barrier discharge plasma: N_2 in the mix as a helping hand or problematic impurity?, Energy & Environmental Science 9(3) (2016) 999-1011.
[60] T. Ohsaka, F. Izumi, Y. Fujiki, Raman spectrum of anatase, TiO_2, Journal of Raman Spectroscopy 7(6) (1978) 321-324.
[61] E.C. Neyts, A. Bogaerts, Understanding plasma catalysis through modelling and simulation—a review, Journal of Physics D: Applied Physics 47(22) (2014) 224010.
[62] K. Van Laer, A. Bogaerts, Fluid modelling of a packed bed dielectric barrier discharge plasma reactor, Plasma Sources Science and Technology 25(1) (2015) 015002.
[63] W. Wang, H.-H. Kim, K. Van Laer, A. Bogaerts, Streamer propagation in a packed bed plasma reactor for plasma catalysis applications, Chemical Engineering Journal 334 (2018) 2467-2479.
[64] Y.-R. Zhang, E.C. Neyts, A. Bogaerts, Influence of the Material Dielectric Constant on Plasma Generation inside Catalyst Pores, The Journal of Physical Chemistry C 120(45) (2016) 25923-25934.